ORIGINAL ARTICLE

Altered microtubule dynamics and vesicular transport in mouse and human MeCP2-deficient astrocytes

Chloé Delépine[1,2,3], Hamid Meziane[4,5,6,7,8], Juliette Nectoux[1,2,3,9], Matthieu Opitz[1,2,3], Amos B. Smith[10], Carlo Ballatore[10,11], Yoann Saillour[1,2,3], Annelise Bennaceur-Griscelli[12], Qiang Chang[13], Emily Cunningham Williams[13], Maxime Dahan[14], Aurélien Duboin[14,15], Pierre Billuart[1,2,3], Yann Herault[4,5,6,7,8] and Thierry Bienvenu[1,2,3,9,*]

[1]Inserm, U1016, Institut Cochin, Paris, France, [2]Cnrs, UMR8104, Paris, France, [3]Université Paris Descartes, Sorbonne Paris Cité, Paris, France, [4]Institut Clinique de la Souris (ICS), PHENOMIN, GIE CERBM, Illkirch, France, [5]Institut de Génétique et de Biologie Moléculaire et Cellulaire, Illkirch, France, [6]Centre National de la Recherche Scientifique, UMR7104, Illkirch, France, [7]Institut National de la Santé et de la Recherche Médicale, U964, Illkirch, France, [8]Université de Strasbourg, Illkirch, France, [9]Laboratoire de Biologie et Génétique Moléculaires, HUPC, Hôpital Cochin, Paris, France, [10]Department of Chemistry, University of Pennsylvania, Philadelphia, PA, USA, [11]Center of Neurodegenerative Disease Research, University of Pennsylvania, Philadelphia, PA, USA, [12]ESTeam Paris-Sud, Université Paris-Sud 11, Inserm U935, Villejuif, France, [13]Department of Genetics and Neurology, University of Wisconsin-Madison, Madison, WI, USA, [14]Laboratoire Physico-Chimie Curie, Institut Curie, CNRS UMR168, UPMC, Paris, France and [15]ALVEOLE, Paris, France

*To whom correspondence should be addressed at: Université Paris Descartes, Institut Cochin, 24 rue du Faubourg St Jacques, 75014 Paris, France. Tel: +33 1 44 41 24 79; Fax: +33 58 41 15 80; Email: thierry.bienvenu@inserm.fr

Abstract

Rett syndrome (RTT) is a rare X-linked neurodevelopmental disorder, characterized by normal post-natal development followed by a sudden deceleration in brain growth with progressive loss of acquired motor and language skills, stereotypic hand movements and severe cognitive impairment. Mutations in the methyl-CpG-binding protein 2 (*MECP2*) cause more than 95% of classic cases. Recently, it has been shown that the loss of Mecp2 from glia negatively influences neurons in a non-cell-autonomous fashion, and that in *Mecp2*-null mice, re-expression of Mecp2 preferentially in astrocytes significantly improved locomotion and anxiety levels, restored respiratory abnormalities to a normal pattern and greatly prolonged lifespan compared with globally null mice. We now report that microtubule (MT)-dependent vesicle transport is altered in *Mecp2*-deficient astrocytes from newborn Mecp2-deficient mice compared with control wild-type littermates. Similar observation has been made in human *MECP2* p.Arg294* iPSC-derived astrocytes. Importantly, administration of Epothilone D, a brain-penetrant MT-stabilizing natural product, was found to restore MT dynamics in *Mecp2*-deficient astrocytes and in *MECP2* p.Arg294* iPSC-derived astrocytes *in vitro*. Finally, we report that relatively low weekly doses of Epothilone D also partially reversed the impaired exploratory behavior in *Mecp2*$^{308/y}$ male mice. These findings represent a first step toward the validation of an innovative treatment for RTT.

Introduction

Rett syndrome (RTT, MIM 3127750) is a rare X-linked neuro-developmental disorder, characterized by seemingly normal post-natal development until ∼6–18 months of age followed by a sudden deceleration in growth with progressive loss of acquired motor and language skills, stereotypic hand movements, major breathing irregularities, electroencephalogram abnormalities, autistic-like behaviors, increased anxiety-like behaviors, sleep disorders and severe cognitive impairment [1,2]. Mutations in the methyl CpG binding protein 2 gene (*MECP2*) cause more than 95% of classic cases [3–5]. *MECP2* encodes a multifunctional protein that binds to methylated DNA and mainly acts as a key transcriptional regulator [2,4]. How mutations in the *MECP2* gene lead to the neurobehavioral features of RTT is still unknown and there is no specific cure for this devastating disorder.

Several lines of mice carrying *Mecp2* disruption are now available. Shortly after the creation of Mecp2-null mice, a mouse expressing a truncated form of Mecp2 (*Mecp2*[308]) has been generated as this type of mutation is commonly found in classic RTT [6]. *Mecp2*[308] mice exhibit behavioral symptoms that recapitulate human RTT phenotype. Interestingly, male *Mecp2*[308/y] mice present RTT phenotype earlier than females and thus are predominantly used in RTT studies [6–9].

More recently, induced pluripotent stem cells (iPSC) from patient carrying common mutation in *MECP2* have been described and characterized [10–19]. RTT iPSC clonal lines and their derived cells stably maintained X-chromosome inactivation (XCI); therefore, the RTT iPSC clonal lines express either the wild-type or the mutant allele of *MECP2* and can be studied as isogenic pairs [12,20]. Methods to efficiently differentiate iPSC into neural progenitor cells, neurons and/or astrocytes have been reported and provide *in vitro* models of human RTT neural cells [21].

Earlier studies suggested the idea that RTT is due exclusively to the loss of Mecp2 function in neurons, because Mecp2 was exclusively present in neurons, based on immunohistochemical analyses. However, several subsequent studies showed that Mecp2 is clearly detected by immunostaining in all glial cell types including astrocytes and oligodendrocytes, based on co-staining for the cell-specific markers (GFAP, NG2 and myelin) [20,22–24]. Using an *in vitro* co-culture system, it has been shown that mutant astrocytes from the knock-out RTT mouse model, and their conditioned medium, fail to support normal dendritic morphology of either wild-type or mutant hippocampal neurons [20]. Although defective neurons clearly underlie the aberrant behaviors, these data suggested that the loss of Mecp2 from astrocytes negatively influences neurons in a non-cell-autonomous fashion [20]. In Mecp2-null mice, re-expression of Mecp2 preferentially in astrocytes significantly improved locomotion, anxiety levels and respiratory abnormalities and greatly prolonged lifespan compared with globally null mice [24]. These data showed that astrocytes, like neurons, are integral components of the neuropathology of RTT. However, only few reports have studied the pathogenic mechanism of RTT astrocytes.

Microtubules (MTs) play a crucial role in many cellular processes, such as cellular morphology, cellular division, migration and intracellular transportation of vesicles. MTs are highly dynamic tubular structures composed of α- and β-tubulin dimers, and their constant polymerization and depolymerization is tightly regulated in the cell. In assembled MTs, acetylation of the lysine-40 of the α-tubulin subunit is a post-translational modification that is often employed as a marker for stable MTs, although the relationship between tubulin acetylation and MT stability is not completely understood [25,26]. Acetylation of

tubulin is mediated by acetyltransferase, while deacetylation is mediated by histone deacetylase 6 (HDAC6) and sirtuin 2 (SIRT2). Recently, we have shown that skin fibroblasts from RTT patients with various mutations in *MECP2* present an altered MT stability in response to cold-induced depolymerization and recovery [27]. The link between MT dynamics impairment and Mecp2 deficiency has been reinforced by the observation of a reduced acetylation of polymerized tubulin and an elevated level of tubulin deacetylase HDAC6 in fibroblasts from RTT patients and in neurons from *Mecp2*-null mice [27,28]. Interestingly, a reduced MT-dependent transport of vesicles containing BDNF in neurons from *Mecp2*-null animals has been reported, highlighting the potential perturbation of cellular functions by Mecp2 deficiency-related impairment of MT dynamics [29]. We previously showed that astrocytes from *Mecp2*[308/y] and *Mecp2*-null mice have a dramatic increase in MT growth rate [30]. However, tubulin acetylation, HDAC6 expression and MT-dependent vesicular transport had not been studied yet in astrocytes.

In this report, we show that astrocytes from *Mecp2*[308/y] mice and human astrocytes derived from iPSC from an RTT patient with an *MECP2* p.Arg294* mutation have a reduced tubulin acetylation, an increase in HDAC6 level, an altered MT dynamics and an MT-dependent cellular dysfunction such as vesicular transport. We show further that MT dynamics impairment in mouse and human Mecp2-deficient astrocytes was counteracted *in vitro* by a treatment with an MT-stabilizing natural product, Epothilone D (EpoD). Finally, treatment with EpoD improved the exploratory behavior in *Mecp2*[308/y] hemizygous male mice. Overall, through this study, we have validated MTs as a target for therapeutic intervention in Rett syndrome, offering a new strategy for treating this disease by modifying stability of MTs by MT-stabilizing natural products.

Results

Astrocytes from Mecp2[308/y] mice have a reduced level of acetylated-tubulin and an increased level of HDAC6

The levels of acetylated tubulin, total tubulin and HDAC6 proteins in total proteins extract from confluent cultures of *Mecp2*[308/y] and wild-type astrocytes were measured by western blot in three independent experiments. A total of six wild-type and six *Mecp2*[308/y] biological replicates were included in the analysis. *Mecp2*-deficient astrocytes showed a decreased level of acetylated tubulin (0.70× ± 0.10; P-value = 0.03) and an increased level of HDAC6 protein (1.73× ± 0.13; P-value = 0.02) when compared with wild-type astrocytes (Fig. 1A and B). Total tubulin level from *Mecp2*-deficient and wild-type astrocytes was similar (Fig. 1A). To determine whether HDAC6 is differentially expressed at the transcriptional level, we measured the mRNA expression by quantitative RT–PCR. HDAC6 mRNA level was not significantly different between *Mecp2*-deficient and wild-type astrocytes (Fig. 1C). Our data suggest that the elevated HDAC6 correlated with a decrease in acetylated-tubulin in Mecp2-deficient astrocytes.

MECP2 p.Arg294* iPSC-derived NPC and astrocytes present a reduced α-tubulin acetylation

To determine whether human astrocytes also presented a reduced α-tubulin acetylation, we examined human astrocytes from isogenic RTT iPSC lines. The iPSC isogenic lines were generated in Pr. Q. Chang Lab from a 11-year-old RTT girl carrying an *MECP2* p.Arg294* mutation, a mutation found in ∼5–6% of RTT
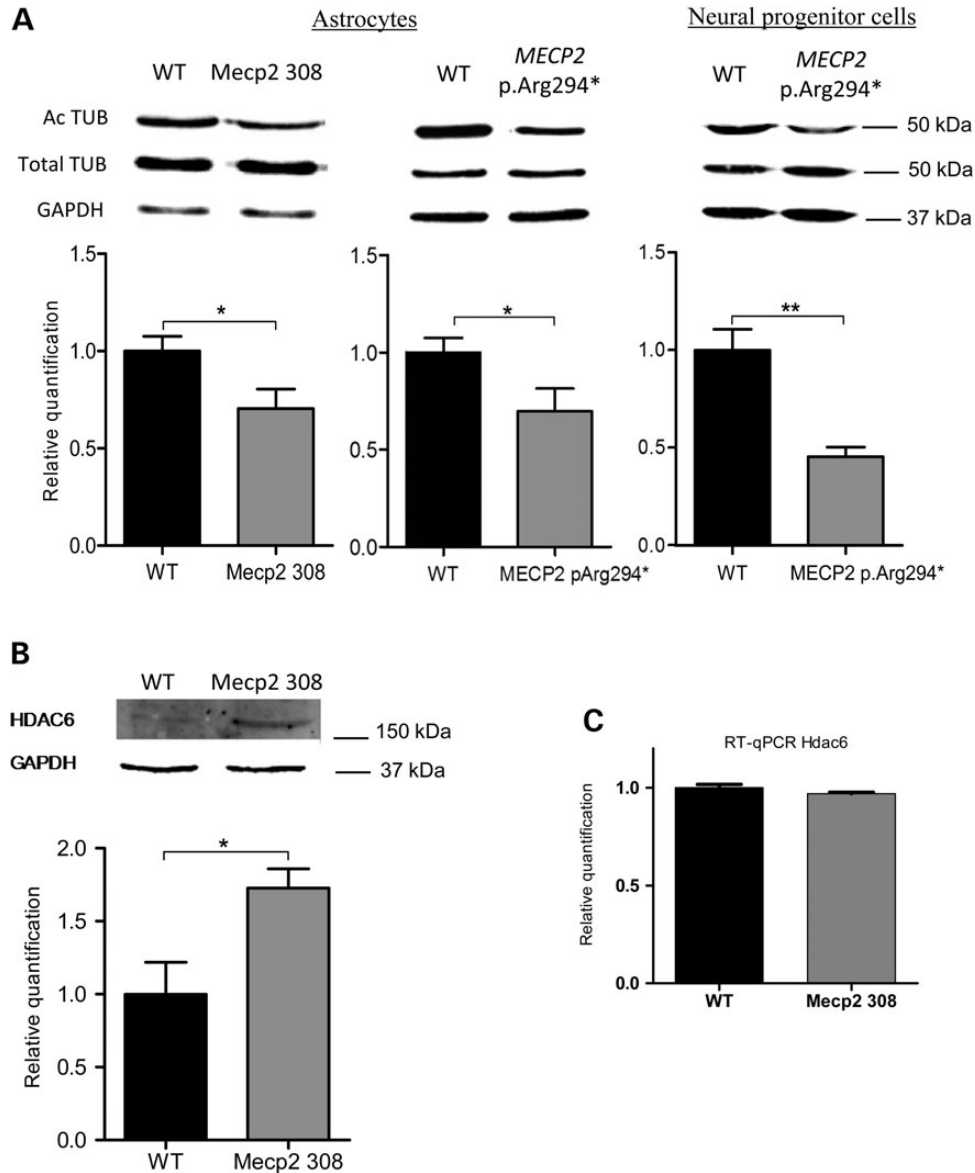
Figure 1. Acetylated-tubulin level is reduced in mouse *Mecp2$^{308/y}$* astrocytes and in human *MECP2* p.Arg294* neural progenitors and astrocytes and associated with an increased HDAC6 protein level in *Mecp2$^{308/y}$*astrocytes. (**A**) Acetylated (Ac TUB) and total tubulin (Total TUB) protein expression levels determined by western blot analysis in *Mecp2*-deficient (Mecp2 308), *MECP2* p.Arg294* and wild-type (WT) astrocytes. (**B**) HDAC6 protein expression level determined by western blot analysis and (**C**) *Hdac6* mRNA level determined by qRT–PCR (right) in *Mecp2*-deficient (Mecp2 308) and wild-type (WT) astrocytes. Normalization of relative quantification of mRNA or protein levels was based on housekeeping *Gapdh* gene and protein. Bars represent means ± SEM. *A P-value for Student's test under 0.05, **A P-value under 0.01.

patients (12). Each line expressed exclusively *MECP2* p.Arg294* mutant or wild-type *MECP2* allele. The quality of iPSC lines was assessed by karyotyping and teratoma-based *in vivo* differentiation assay. The iPSC lines had normal karyotype and, after transplantation *in vivo*, gave rise to cells of the three germ layers (Supplementary Material, Fig. S1). From the two isogenic iPSC lines, we generated neuroepithelial cells with dorsal forebrain regional identity as described previously (31). No difference in the ability of the two isogenic lines to form neural tube-like rosettes was observed. The iPSC differentiation into neural subtypes was monitored by immunostaining for several known markers (Supplementary Material, Fig. S2A). As assessed by quantitative RT–PCR, at 8 weeks of differentiation, *MECP2* p.Arg294* and wild-type astrocytes were expressing astrocyte markers at significant levels (Supplementary Material, Fig. S2B). Astrocytes

used for further phenotypic characterization were then at 6–10 weeks of differentiation from iPSC. The XCI status and *MECP2* allelic expression of astrocytes derived from the iPSC lines were tested to validate the maintenance of their isogenic status. After digestion with methylation-sensitive enzymes, a different androgen receptor hypermethylated allele was amplified in the two iPSC lines with a totally skewed X chromosome inactivation (Supplementary Material, Fig. S3). Moreover, sequencing of *MECP2* allele-specific expression showed that iPSC and astrocytes of the same line expressed only the expected wild-type or mutated *MECP2* p.Arg294* allele (Supplementary Material, Fig. S3). Human isogenic astrocytes expressing either exclusively the *MECP2* p.Arg294* or the wild-type *MECP2* allele were produced at the same time from iPSC being at the same passage. At least three independent differentiation experiments from separate

iPSC passages were performed to provide the astrocytes tested for the following experiment replicates.

Total proteins were extracted from *MECP2* p.Arg294*and wild-type NPCs and astrocytes pairs from four separate differentiations (6–10 weeks of differentiation). The levels of acetylated α-tubulin in *MECP2* p.Arg294*cells were significantly lower than in the corresponding isogenic wild-type pair (0.70× ± 0.07; *P*-value = 0.04), whereas no difference in total α-tubulin level was observed (Fig. 1A). As we observed in *Mecp2*-deficient astrocytes from mice, a decreased level of acetylated-tubulin was then confirmed in the human RTT iPSC-derived astrocytes.

Astrocytes from Mecp2[308/y] mice present larger EB3 localization at the MT plus-end

To examine the possibility that Mecp2 plays a role in the stability of the cytoskeleton in astrocytes, we performed MT dynamics assay in astrocytes from *Mecp2*[308/y] mice and their control wild-type littermates. Cells were transfected by tracking 'comets' of MT-plus-end binding proteins EB3 fused to GFP (32). Our previous

report showed a significant increase in MT polymerization speed in *Mecp2*-deficient astrocytes (30). Previous report showed that inhibition of HDAC6 activity in CHO cells has been associated with a decrease in MT growth velocity and a shorter binding site of proteins accumulating at growing MT tip (33). To determine if the elevated HDAC6 expression and the increased MT growth velocity in *Mecp2*[308/y] astrocytes were associated with accumulation of MT-tip proteins on growing MTs, we measured the size of EB3-comet and observed as postulated that EB3-labeled tails size was larger in *Mecp2*[308/y] astrocytes than in wild-type astrocytes (0.503 ± 0.018, *n* = 42; 0.580 ± 0.015, *n* = 38; *P*-value = 0.002) (Fig. 2) reinforcing the idea that MT stability is affected in Mecp2 deficiency.

MECP2 p.Arg294* iPSC-derived astrocytes present a high MT growth velocity and large EB3 MT-binding area

Taking account that cell shape is an essential factor governing MT organization and dynamics and to avoid the high variability in human astrocytes morphology, we choose to obtain a population of human astrocytes with homogeneous morphologies
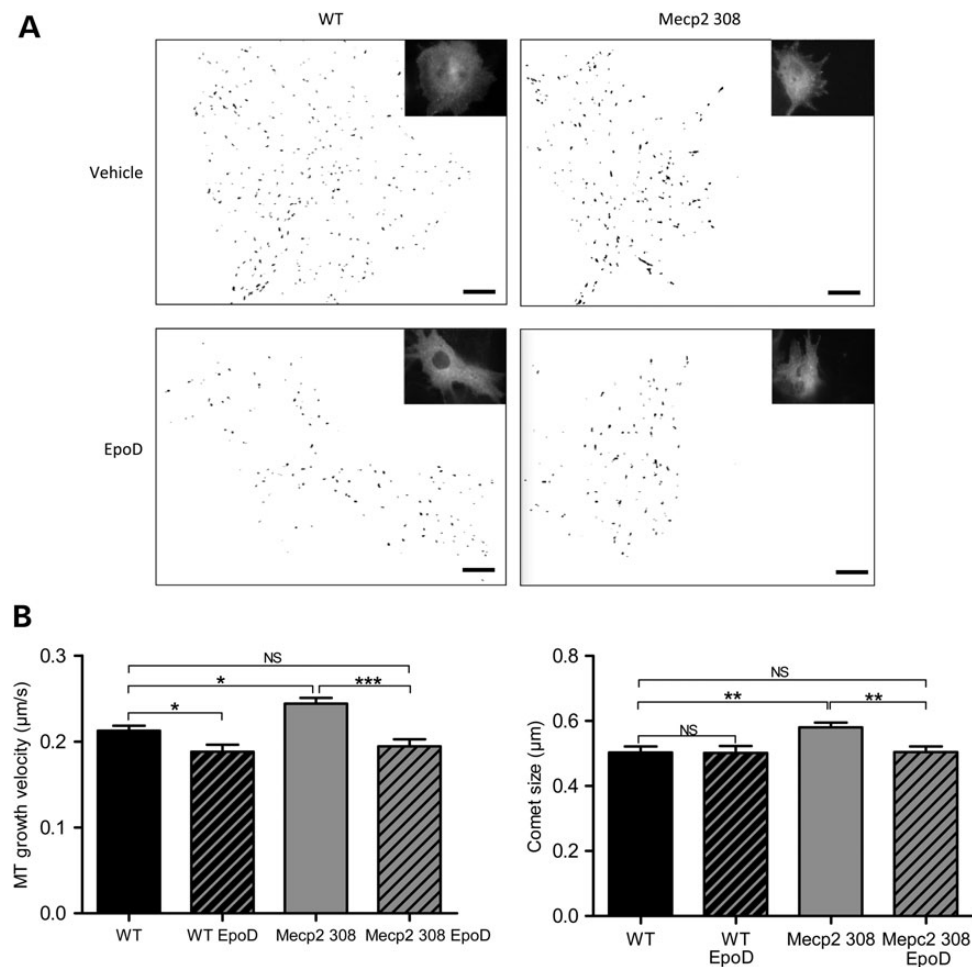

Figure 2. Mouse *Mecp2*[308/y] astrocytes present an increased MTs growth velocity and an increased EB3-comet size in comparison with wild-type astrocytes that can be normalized by EpoD treatment. EB3-GFP transfected wild-type (WT) and Mecp[308/y] (Mecp2 308) astrocytes were incubated with 10 nM EpoD or vehicle for 1 h before measurement. EB3-GFP movement corresponding to MTs plus end growing radially from the centrosome region was followed in single cells by time-lapse microscopy (image acquisition every 1 s during 1 min, 61 images) and EB3-GFP velocity and comet size were measured. A total of 42 WT, 38 Mecp2[308/y] cells treated with vehicle and 15 WT and 27 Mecp2[308/y] cells treated with EpoD were included in the analysis. About 100 comets were tracked in each cell. (**A**) Representative illustrations of the comet-like labeling of MT plus ends EB3-GFP in astrocytes and the associated binary (black and white) images. Scale bar represents 10 μm. (**B**) Histograms of MT growth velocity (left) and EB3 comet size (right). Bars represent means ± SEM. *A *P*-value for Student's test under 0.05, **A *P*-value for Student's test under 0.01, ***under 0.001, NS a *P*-value over 0.05.

by using non-adherent poly-ʟ-lysine-polyethylene glycol (PLL-PEG)-coated coverslips patterned with adherent 40 µm large fibronectin lines. Cell morphology was homogenized into polarized longitudinal cells (Fig. 3). Astrocytes were transfected with EB3-GFP construct for 24 h before EB3 tracking as previously described (32). Similarly to mouse Mecp2-deficient astrocytes, *MECP2* p.Arg294* astrocytes showed a significantly higher MT growth velocity compared with isogenic wild-type astrocytes (0.285 ± 0.011, *n* = 28; 0.339 ± 0.008, *n* = 46; *P*-value

<0.001) (Fig. 3). Moreover, the mean EB3 comet size was also significantly larger in *MECP2* p.Arg294* astrocytes than in the wild-type human astrocytes (0.448 ± 0.022, *n* = 28; 0.697 ± 0.038, *n* = 46; *P*-value <0.0001) (Fig. 3). These data show that MT stability is affected by Mecp2 deficiency both in mouse and human astrocytes.

Astrocytes from mouse Mecp2$^{308/y}$ and human *MECP2* p. Arg294* iPSC-derived astrocytes present an altered directionality of vesicle transport.
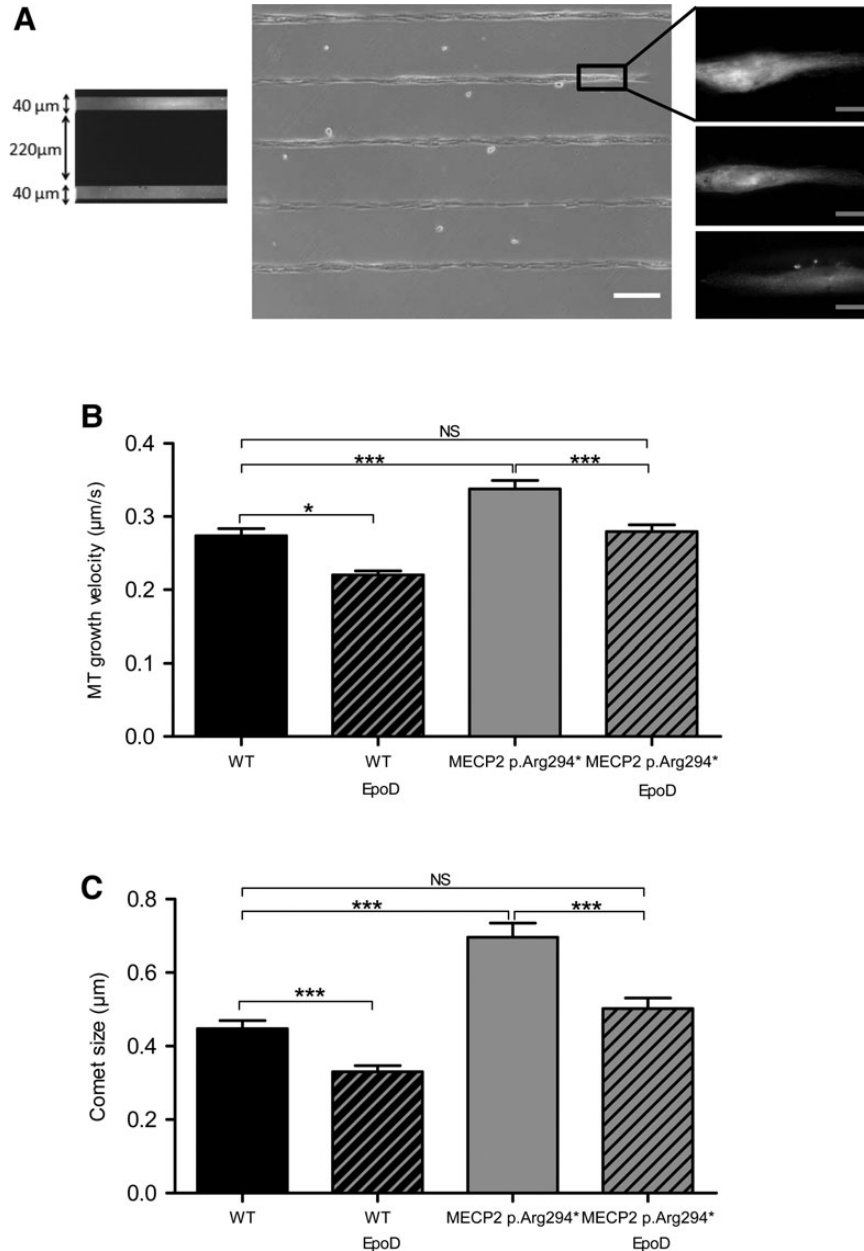

Figure 3. Human *MECP2* p.Arg294* astrocytes present a higher MT growth velocity and a higher EB3-comet size than wild-type astrocytes in standardized morphology condition, that can both be corrected by EpoD. (**A**) Cells were seeded on PLL-PEG-coated coverslips printed with 40 µm large lines of fibronectin and presented subsequently a homogeneous polarized morphology. Fluorescent fibronectin lines are shown in the left panel. The middle panel illustrates the cell alignment on fibronectin lines (white light) and the right panel gives examples representative of the homogeneous morphology adopted by the EB3-GFP expressing cells prior to time-lapse microscopy. (**B** and **C**) EB3-GFP transfected wild-type (WT) and *MECP2* p.Arg294* isogenic astrocytes were incubated with 10 nᴍ EpoD or vehicle for 1 h before timelapse imaging. EB3-GFP movement corresponding to MTs end growing radially from the centrosome region was followed in single cells by time-lapse microscopy (image acquisition every 1 s during 1 min, 61 images) and EB3-GFP velocity and comet size were measured. A total of 28 WT, 46 *MECP2* p.Arg294* vehicle-treated cells, 8 WT and 36 *MECP2* p.Arg294* EpoD-treated cells were included in the analysis. Bars represent (B) mean EB3 comet velocity and (C) mean EB3 comet size, ± SEM. *A P-value for Student's test under 0.05, ***under 0.001 and NS over 0.05. White scale bar represents 200 µm, gray scale bar represents 10 µm.

To determine if MT-dependent vesicle transport was affected by MT dynamics defect in mouse *Mecp2*[308/y] and human *MECP2* p. Arg294* astrocytes, and as lysosome vesicles are transported along MTs, we measured the fraction of highly directional versus highly non-directional (ND) mobile lysosome vesicles as described previously (34). Astrocytes cultures were incubated with Lysotracker® and Lysotracker-positive lysosome vesicles were tracked during 2 min movies with a picture acquisition every 2 s. As previously described, vesicles were classified as mobile vesicles by the criteria of a track length over 1 μm (35). Lysotracker-positive mobile vesicles displayed complex motion patterns composed of forward and backward movements interrupted by periods of arrested mobility. We distinguished vesicles moving in a highly directional fashion and vesicles moving in a highly ND fashion by taking account of the ratio of the displacement, meaning the distance between the first and the last spot position, over the total track length of each mobile vesicle. Vesicles with a displacement under 20% of the total track length were classified as highly ND. Around 100–200 vesicles were tracked per cell. Interestingly, Mecp2 deficiency in astrocytes from both models is associated with a slight but significant and reproducible increase in vesicles moving in a highly ND fashion when compared with wild-type astrocytes [mouse astrocytes: 46.93% ± 2.18, $n = 55$; 55.59% ± 3.67, $n = 64$; P-value 0.04 (Fig. 4A); human astrocytes: 37.96% ± 1.92, $n = 57$; 46.70% ± 1.86, $n = 74$; P-value = 0.001 (Fig. 4B)]. Our data showed for the first time that MT-dependent vesicle mobility is altered in Mecp2-deficient astrocytes.

Epothilone D treatment of mouse Mecp2[308/y] and human MECP2 p.Arg294* iPSC-derived astrocytes rescues MT growth velocity and EB3-comet size

To investigate the ability of Epothilone D (EpoD) (36), an MT-stabilizing natural product, to correct the impaired cellular phenotype observed on RTT astrocytes, mouse and human *MECP2*-deficient astrocytes and wild-type astrocytes cultures were incubated with EpoD at a concentration of 10 nM or with vehicle before performing EB3-GFP. *Mecp2*[308/y] and wild-type astrocytes treated with EpoD presented a reduced EB3-comet speed (0.213 ± 0.006, $n = 42$; 0.188 ± 0.008, $n = 15$; P-value = 0.02; 0.244 ± 0.007, $n = 38$; 0.194 ± 0.008, $n = 27$; P-value < 0.001) and size (0.580 ± 0.015, $n = 38$; 0.505 ± 0.017,

$n = 27$; P-value = 0.002) (Fig. 2). Similarly, the effect of EpoD treatment on human wild-type and *MECP2* p.Arg294*isogenic astrocytes was a reduction in EB3-GFP velocity (0.285 ± 0.011, $n = 28$; 0.220 ± 0.005, $n = 8$; P-value = 0.02; 0.339 ± 0.008, $n = 46$; 0.279 ± 0.009, $n = 36$; P-value = 0.0004) and EB3-GFP comet size (0.448 ± 0.022, $n = 28$; 0.337 ± 0.016, $n = 8$; P-value = 0.0002; 0.697 ± 0.038, $n = 46$; 0.502 ± 0.029, $n = 36$; P-value = 0.0003) (Fig. 3). Moreover, the growth velocity of MTs (mouse astrocytes: 0.213 ± 0.006, $n = 42$; 0.188 ± 0.008, $n = 27$; P-value = 0.119; human astrocytes: 0.285 ± 0.011, $n = 28$; 0.279 ± 0.009, $n = 36$; P-value = 0.69) and EB3-comet size (mouse astrocytes: 0.502 ± 0.021, $n = 42$; 0.505 ± 0.017, $n = 27$; P-value = 0.93; human astrocytes: 0.448 ± 0.022, $n = 28$; 0.502 ± 0.029, $n = 36$; P-value = 0.14) were not significantly different between Mecp2-deficient astrocytes treated with EpoD and wild-type astrocytes treated with vehicle (Figs. 2 and 3).

Epothilone D treatment of mouse Mecp2[308/y] astrocytes rescues vesicle directionality

Mouse Mecp2[308/y] astrocytes were treated with 10 nM EpoD for 1 h before performing lysosomes tracking. *Mecp2*[308/y] and wild-type astrocytes treated with EpoD presented a reduced percentage of vesicles moving in a highly ND fashion (46.93% ± 2.18, $n = 55$; 39.07% ± 3.57, $n = 15$; P-value = 0.04; 55.59% ± 3.67, $n = 64$; 46.04% ± 3.14, $n = 17$; P-value = 0.04) in comparison with *Mecp2*[308/y] and wild-type astrocytes treated with vehicle, respectively. Vesicle directionality (46.93% ± 2.18, $n = 55$; 46.04% ± 3.14, $n = 17$; P-value = 0.81) was not significantly different between Mecp2-deficient astrocytes treated with EpoD and wild-type astrocytes treated with vehicle (Fig. 4). Thus, EpoD is able to rescue the vesicle directionality in Mecp2-deficient astrocytes *in vitro* (Fig. 4). These data also show that acting on MT dynamics results in a modulation of lysosome vesicle directionality, reinforcing the idea that impairment of MT dynamics leads to vesicular trafficking alteration in RTT.

Epothilone D corrects exploratory behavioral symptoms of Mecp2[308/y] male mice

Prior pharmacokinetic studies revealed that EpoD has significantly longer resistance time in the brain than in plasma of mice (36), the compound being detectable in brain for at least 1
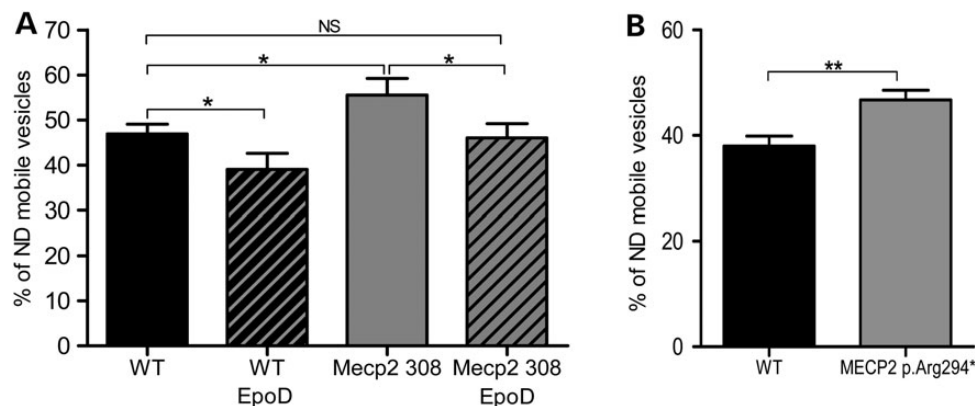

Figure 4. Lysosome vesicle directionality is altered in mouse *Mecp2*[308/y] and human *MECP2* p.Arg294* astrocytes and is rescued by EpoD treatment in mouse *Mecp2*[308/y] astrocytes. Cells were incubated 1 h with 200 nM LysoTracker® and 10 nM EpoD or vehicle before timelapse imaging. For each vesicle, displacement length (DL) and total track length (TL) were measured by Imaris Software (Bitplane). Vesicle was considered mobile when its total track length was >1 μm and ND when its DL/TL ratio was <20%. We tracked 100–200 vesicles per cell. (**A**) A total of 55 WT, 64 *Mecp2*[308/y] vehicle-treated cells, 15 WT and 17 *Mecp2*[308/y] EpoD-treated cells were analyzed. (**B**) A total of 57 WT, and 74 *MECP2* p.Arg294* cells were analyzed. Bars represent mean proportion of ND mobile vesicles by cell ± SEM.*A P-value for Student's test under 0.05, NS a P-value over 0.05.
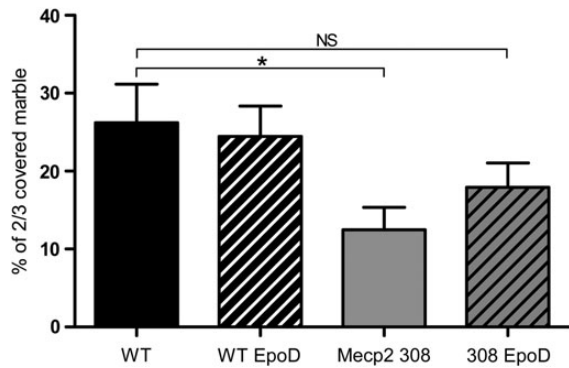
Figure 5. EpoD corrects Mecp2[308/y] mice performance in the marble-burying test. Proportion of 2/3 covered marbles in the marble-burying test. Bars represent mean ± SEM. *A P-value for Student's test under 0.05, NS a P-value over 0.05.

week after a single 3 mg/kg administration. Moreover, a measurable pharmacodynamics effect was apparent 1 week after a single 3 mg/kg dose of EpoD to wild-type mice, as evidenced by increased levels of acetylated-tubulin (37). In a previous behavioral study, it has been clearly demonstrated that *Mecp2[308/y]* mice displayed decreased digging and buried a lower number of marbles compared with wild-type littermates in the marble-burying test (9). Here, based on this study and our *in vitro* data, we investigated EpoD effects on exploratory behavior in an RTT mouse model. Five-weeks-old *Mecp2[308/y]* mice were treated by weekly intraperitoneal injection of EpoD (1 mg/kg/week). To evaluate the effects of EpoD on exploratory behavior, the marble-burying test was carried out on a 12-week treatment schedule. As expected, *Mecp2[308/y]* mice buried a lower proportion of 2/3 covered marbles compared with wild-type littermates (26.20% ± 4.95, $n = 7$; 12.49% ± 2.87, $n = 9$; P-value = 0.02), indicating decreased environment-directed exploratory behavior (Fig. 5). Proportion of 2/3 covered marbles buried by the EpoD-treated *Mecp2[308/y]* mice was not significantly different from that of wild-type mice (26.20% ± 4.95, $n = 7$; 17.93% ± 3.11, $n = 10$; P-value = 0.16), thus suggesting that treatment of *Mecp2[308/y]* mice with EpoD restored the impaired exploratory behavior (Fig. 5).

Discussion

MTs are highly dynamics structures and the regulation of MTs dynamics is crucial for cellular functions such as migration, division, polarity and differentiation. The MTs plus-ends display what is called MT instability, which is the succession of slow polymerization and fast depolymerization events, essential for MTs to explore the cell. MTs are polymers of basic α/β-tubulin dimer building units. It is not clear how the functional diversity of MTs is created. One growing hypothesis is that post-translational modifications of tubulin regulate MT functions. Among them, the acetylation of α-tubulin at lysine 40 is found on stable MTs in most cell type. Although the relationship between tubulin acetylation and MT stability is not completely understood, acetylated-tubulin is often considered as a marker for stable MTs. However, this post-translational modification has been reported to play a positive role in motor-based trafficking (27,38–41). Two enzymes have been shown to deacetylate α-tubulin *in vitro* and *in vivo*, HDAC6 and SIRT2 (42,43). Based on our and other previous works reporting that astrocytes, like neurons, are integral components of the neuropathology of

RTT, we focus our study on astrocytes (17,20,22–24). We have shown for the first time that *Mecp2[308/y]* astrocytes display a low level of tubulin acetylation and overexpress HDAC6 protein. This HDAC6 overexpression was not associated with an increase in HDAC6 mRNA transcript, suggesting that Mecp2 may modulate HDAC6 synthesis and/or degradation at the post-transcriptional level. It is interesting to note that similar observations were recently obtained in Mecp2-deficient fibroblasts and Mecp2-null neurons (28). Notably, HDAC6 modulation was shown to modulate some aspects of MT dynamics, such as MT growth velocity, but not the frequency of catastrophe (transition from growth/pause to shortening) and rescue (transition from shortening to growth/pause) events, or the time spent in growing, shortening and pausing (33). We thus focused on this parameter of MT dynamics and observed that *Mecp2*-deficient astrocytes display increased MT growth velocity. Moreover, HDAC6 activity has been shown to modulate the localization of the plus-end-tracking protein EB1 and Arp1 at the MTs tip (33). We have shown that EB3-GFP comet tail was larger in the *Mecp2*-deficient astrocytes, which is likely associated with HDAC6 protein overexpression.

Potokar *et al.* (34,44) have demonstrated the contribution of MTs to directional vesicle mobility in astrocytes. In line with those studies, we showed that altered MT dynamics in *Mecp2*-deficient astrocytes from *Mecp2[308/y]* mice affects the directional mobility of vesicles. Indeed, distinct types of vesicle mobility have been described in astrocytes, consistent with other cell types: a slow and disorganized diffusion transport and an MT-dependent fast and straight trafficking (34). Vesicles were characterized as highly directional when vesicle tracks displaying a straight line and highly ND when vesicle tracks displaying a contorted line. Interestingly, we observed that the percentage of highly directional vesicles is reduced in *Mecp2[308/y]* astrocytes compared with wild-type astrocytes. An efficient vesicle cellular transport is necessary for cell function and vesicle exocytosis. As exocytosis from astrocytes is essential in astrocyte-to-neuron communication, our results suggest that altered MT dynamics and vesicle trafficking in Mecp2-deficient astrocytes may lead to an impaired astrocyte secretion that may contribute to the neuronal maturation defect observed in *Mecp2*-deficient brains. Previous reports have also shown that Mecp2 deficiency impairs axonal transport of amyloid precursor protein without affecting its mRNA and protein levels, and that Mecp2 knockout neurons have fewer fast-moving mitochondria than wild-type neurons (29,45). Those data together suggest that Mecp2 deficiency affects the global MT-dependent transport.

Interestingly, we found in the human *MECP2* p.Arg294* isogenic iPSC-derived astrocytes a phenotype similar to the one found in *Mecp2*-deficient mouse primary culture. It will be of interest to study human astrocytes derived from more RTT patients, with different mutations in *MECP2* gene. However, our results highlight the value of iPSC-derived cells as a good model to study Rett syndrome physiology and validate that MT dynamics may be affected in RTT patient cerebral cells and could be a putative target for RTT therapy.

Tubulin acetylation and MT dynamics alteration in *Mecp2*-deficient cells have been highlighted by our study and others in cerebral cells from three different *Mecp2*-deficient mice models and in human cells from male and female RTT patients with different mutations in *MECP2* genes, providing a robust Mecp2 deficiency-linked cellular phenotype. However, the links between Mecp2 deficiency with impaired tubulin acetylation and increased MT instability have to be further studied to better understand the cause–effect relationships between those cellular

events. We suggest that altered MT dynamics leads to an impairment of cellular functions in astrocytes, which may participate in the pathogenic state of *Mecp2*-deficient astrocytes and contribute to an altered neuronal maturation.

Treatments of 3T3 cells with HDAC6 inhibitor and MT stabilizer both increase the MTs polymer content and the acetylation level of the MT network, and slow down the drug-induced depolymerization of MTs (42). We show in this report that EpoD, a well-characterized MT stabilizer, can restore both MT dynamics and mobile vesicle directionality in *Mecp2*-deficient astrocytes at a very low concentration. This result indicates that alterations in MT dynamics and mobile vesicle directionality in *Mecp2*-deficient astrocytes are linked and such cellular phenotypes can be corrected with a regulator of MT dynamics. As a result, MTs comprise a potentially promising target for RTT therapy.

De Filippis *et al*. (9) recently described that *Mecp2*[308/y] mice had a decreased marble-burying behavior that may reflect an impairment of the environment-directed exploratory behavior. This phenomenon was accompanied by increased anxiety and by the absence of spontaneous stereotypic behavior. The performance of RTT mice in the marble-burying test was restored in this study by a selective brain-penetrant agonist (LP-211) treatment, suggesting the reversibility of this Mecp2[308]-associated phenotype (9). Consistent with these observations, when we employed the marble-burying test, we also noted that *Mecp2*[308/y] mice harbored an altered exploratory behavior. Taking account our *in vitro* results, we studied the effect of an MT-stabilizing molecule *in vivo* in *Mecp2*[308/y] mice. Because paclitaxel, a drug acting against MT depolymerization through its binding to β-tubulin, is not suitable for human neurodevelopmental disorders because of poor blood–brain barrier (BBB) permeability, we evaluated the effects of a brain-penetrant MT-stabilizing natural product, EpoD. Moreover, EpoD has been shown to improve behavior in a mouse model for schizophrenia and Alzheimer-like pathology (46,47). Because RTT patients can only be diagnosed after the beginning of the regression period (9–18 months), we started the mouse treatment on early symptomatic *Mecp2*[308/y] mice (1 month old). Here, we show that EpoD treatment improved the RTT mice exploratory behavior in the marble-burying test. Our data provide the first evidence that a regulator of MT dynamics might have a beneficial effect, opening new possibilities for the development of novel pharmacological approaches for the treatment of Rett syndrome. However, MT-stabilizing agents are known to induce side effects when used at the doses required for the treatment of cancer. Hence, it is important to note that the aged mice in this study received EpoD doses that were 30- and 100-fold less, on a milligrams per square meter basis, than was previously used in human testing (48). Thus, the substantially lower EpoD doses used here may avoid the adverse complications associated with MT-stabilizing drugs, such as immune cell depletion and the onset of peripheral neuropathy (49). In the present study, the *Mecp2*[308/y] mice receiving EpoD had body weights at the end of the dosing period that were indistinguishable from vehicle-treated wild-type mice, indicating an absence of gross toxicities. Therefore, it appears that the low doses of EpoD used in this study, which were sufficient to improve efficacy outcomes, elicited none of the adverse events that are observed when higher doses of MT-stabilizing agents are used for the treatment of cancer. In conclusion, through this study, we have validated MTs as a target for therapeutic intervention in Rett syndrome, offering a new strategy for treating this disease by modifying stability of MTs by BBB-permeable MT dynamics regulators.

Materials and Methods

Subjects

The experimental subjects were 5 weeks of age hemizygous *Mecp2*[308/y] male mice and wild-type littermates (B6.129S-MeCP2<tm1Heto>/J, stock number: 005439; backcrossed to C57BL/6J mice for at least 12 generations from the Jackson Laboratories, USA) (6). All procedures were carried out in accordance with the new European Communities Council Directive (2010/063 EU) and the implementing French decree of application no 2013-118 01 and its supporting annexes entered into legislation 1 February 2013. All procedures were formally approved by local ethical committees from Paris Descartes University and the Com'Eth (no 17) for the laboratories in Illkirch.

Genotyping

Genotyping was performed by routine PCR technique according to The Jackson Laboratory protocols. The gender was determined using primers for the *Sry* gene on Y chromosome, which were 5′-CTC ATC GGA GGG CTA AAG TG -3′ and 5′-AAG CTT TGC TGG TTT TTG GA-3′. Genotype was determined using primers for the *Mecp2* gene, which were 5′-AAC GGG GTA GAA AGC CTG-3′, 5′-TGA TGG GGT CCT CAG AGC-3′ and 5′-ATG CTC CAG ACT GCC TTG-3′ for *Mecp2*[308/y] mice.

Preparation of EpoD

EpoD was prepared as previously described (50,51). The spectroscopic properties of EpoD were identical to those reported in the literature. Compound purity was >95% as demonstrated by liquid chromatography-mass spectrometry. The compound was dissolved in vehicle solution, i.e. 1% dimethyl sulfoxide (DMSO) in saline.

Cortical mouse astrocyte cultures

Primary astrocyte cultures were prepared from 1-day-old wild-type and Mecp2[308/y] mice, male cerebral cortex according to previously described methods (52). Briefly, after removal of the meninges, forebrains were rinsed and gently dissociated by trituration following 30 min incubation with trypsin 0.05% (Invitrogen, Cergy-Pontoise, France). Cells were collected by centrifugation at 300*g* for 3 min, resuspended in DMEM supplemented with 10% heat-inactivated FBS, plated in micro-dishes designed for live imaging (μ-Dish 35 mm; Ibidi, München, Germany) and incubated at 37°C in a humidified atmosphere of 95% air, 5% CO_2. The purity of the cells, as determined by glial fibrillary acidic protein (GFAP) immunohistochemical staining was >99% (Supplementary Material, Fig. S4). Each experiment was performed with astrocytes primary culture from littermate newborn pups and each litter contained at least two *Mecp2*[308/y] and two wild-type pups.

Human astrocytes production from iPSC

Maintenance of iPSC cultures

iPSC lines from *MECP2* p.Arg294* RTT patient used in this study have been previously described (12). iPSC were amplified with mTeSR1® medium (StemCell Technologies, Grenoble, France) on matrigel (BD Biosciences, Franklin Lakes, NJ, USA) coated dish and passaged with collagenase IV (StemCell Technologies). iPSC were used for astrocyte differentiation at passage ~P30–40.

Astrocyte differentiation

Astrocytes with a dorsal regionalization were produced by iPSC differentiation as previously described (53). Briefly, embryoid bodies were generated from iPSC and neuroectoderm induced by inhibition of BMP4 signaling pathway. Columnar neuroepithelial cells formed typical neural tube-like rosettes. Rosettes were dissociated into monolayer of neural progenitor cells with Neurobasal A medium supplemented with 1×N2, 1× B27 without vitamin A, 1×GlutaMAX, 1× PenStrep (LifeTechnologies, Cergy-Pontoise, France) and 10 ng/ml of FGF-2 (Miltenyi Biotech, Paris, France) and EGF (LifeTechnologies). At day 15 of differentiation, highly proliferating neural progenitor cells were switched to astrogenesis by medium supplementation by human recombinant CNTF (Bio-Techne, Abingdon, UK) and deprivation of FGF-2 and EGF for 2 weeks, then CNTF supplementation was stopped and cells were maintained in culture for months. Most of the experiments were performed on astrocytes at 6–10 weeks of differentiation.

Human androgen receptor assay

XCI status was investigated by sizing the polymorphic CAG trinucleotide repeat on the inactive androgen receptor allele as previously described (54).

Karyotyping

Standard G-banding chromosome analysis was performed in Laboratory of Cytogenetics, GHU Cochin-Broca-Hôtel Dieu, Paris, France.

Teratoma assay

Teratoma formation was assessed by injecting hiPSCs into immunodeficient mice as previously described (55).

Allele-specific transcription of *MECP2*

Total RNA from the iPSC lines and human astrocytes cultures were converted to cDNA with Maxima First Strand cDNA synthesis Kit (ThermoScientific, Rochester, NY, USA). Region containing the mutation was amplified by PCR amplification and sequenced with an ABI 3100® (Applied Biosystems, Courtaboeuf, France). Primer sequences were 5′-ACC GGG GAC CCA TGT ATG AT-3′ and 5′-ATG TCT TTG CGC TCT CCC TC-3′.

Quantitative RT-PCR

Total RNA from the human astrocytes cultures were converted to cDNA with Maxima First Strand cDNA synthesis Kit (Thermo-Scientific) for quantitative real-time PCR with SYBR Green as detection agent with the LightCycler480 detection system (Roche Applied Bioscience, Indianapolis, IN, USA). Primer sequences are described in Supplementary Material, Table S1. After PCR amplification, a dissociation protocol was performed to determine the melting curve of the PCR product. Reactions with melting curves indicating a single amplification product were considered positive for further analysis. The identity and expected size of the single PCR product were also confirmed by agarose gel electrophoresis. Normalization factor was based on housekeeping gene *Gapdh*.

Western blot

The levels of HDAC6, α-tubulin and acetylated α-tubulin protein expression were determined by western blot analysis. Briefly, proteins were extracted from cell cultures in RIPA buffer supplemented with protease inhibitors (Sigma-Aldrich). The protein samples were separated by a 10% sodium dodecyl sulfate–polyacrylamide gel electrophoresis and then transferred to Hybond-C nitrocellulose membrane (GE Healthcare, Piscataway, NJ, USA). After blocking non-specific sites by a TBS-Tween 20 0.05%/5% fat milk solution for 1 h at room temperature, the membrane was incubated overnight at 4°C with a mouse anti-acetylated-tubulin monoclonal antibody (clone 6-11B-1, SIGMA T6793), mouse anti α-tubulin monoclonal antibody (clone DM1A, SIGMA T9026) and goat anti-HDAC6 polyclonal antibody (Santa Cruz Biotechnology sc-5258), washed and incubated with horseradish peroxidase-conjugated secondary antibodies (anti-mouse or anti-goat), and developed with the enhanced chemiluminescence method (ECL; GE Healthcare). We also probed membranes for GAPDH (antibody anti-Gapdh Ambion, dilution 1:1000) for loading normalization. Quantification of protein levels was measured by the chemiluminescence intensity.

Immunostaining

Cells were washed twice with PBS and fixed with paraformaldehyde 4% during 15 min. Cells were incubated in 0.1% Triton and 3% bovine serum albumin solution for 1 h and then incubated with goat anti-GFAP (Santa Cruz Biotechnology, sc-6170), mouse anti-OCT4 (clone C-10, Santa Cruz Biotechnology, sc-5279), rabbit anti-PAX6 (Covance, PRB-278P-100) or mouse anti-S100β (Sigma Aldrich, s2532) antibody overnight. After primary antibody washing, cells were incubated 1 h, respectively, with appropriate chromophore-conjugated secondary antibodies (FITC or CY3, produced in donkey, Jackson Immuno Research) and then mounted with Fluoromount mounting medium with DAPI (Sigma Aldrich, St Louis, MO, USA) and analyzed with a Leica DMRA2 fluorescence microscope.

Adherence proteins micro-patterning

Solutions

A 10× stock solution of poly-ʟ-lysine-poly-ethylene-glycol (PLL-PEG) was prepared dissolving 1 mg/ml of PLL-g-PEG (PLL(20)-[3.5]-PEG(2), SuSoS) in 10 mᴍ HEPES buffer, pH = 7.4, stored at −20°C. By diluting aliquots of the stock solution in the same buffer, 1× solution of PLL-PEG (100 μg/ml) was obtained. Adherent proteins solution was composed of 50 μg/ml of fibronectin (F1141, Sigma-Aldrich) and 50 μg/ml of fibrinogen-Alexa647 (F35200, LifeTechnologies) in 10 mᴍ NaHCO3 buffer, pH 8.3.

Micro-patterning

A 35 mm glass bottom μ-Dish (81158, Ibidi) was treated with oxygen plasma to clean and activate the glass surface, and turn it hydrophilic. Then a 250 μm thick PDMS spacer cut with a plotter-cutter (Craft ROBOProS, Graphtec) was stuck on the glass surface to define four wells of 4 mm diameter. Each well was incubated with 20 μl of a 1× PLL-PEG solution for 1 h to coat the glass surface. After rinsing with PBS 1×, we achieved the micro-patterning of a mix of fibronectin and fibrinogen-Alexa647 on the surface in each well, with a device developed by ALVEOLE coupling an optical system to a chemical product (Primo™ PLPP™, ALVEOLE, Paris, France). We therefore get horizontal lines of 40 μm in width vertically spaced by 220 μm.

Cell seeding

Human astrocytes (6–10 weeks differentiation from iPSC) were seeded on extemporaneously patterned wells at a concentration

of 3000 cells into 10 μl of culture medium. After 1 h, wells were rinsed three times with culture medium to remove non-attached cells and dish was filled with 2 ml of culture medium.

Live cells measurement of MT dynamics

Constructs

The EB3-GFP construct (generously provided by F. Niedergang, Institut Cochin, Paris, France) has been previously described (32). Briefly, gene-specific primers were designed for cloning of *EB3* cDNA, with restriction sites for in-frame cloning after PCR amplification into *pEGFP-N1* (Clontech, Palo Alto, CA, USA). The expression of this vector is driven by CMV promoter.

Transfection of mouse and human astrocytes

Two weeks in vitro confluent mouse astrocyte cultures and 6–10 weeks iPSC-derived human astrocytes were transfected using Lipofectamine LTX (Invitrogen) with EB3-GFP vector. Transfected cells were cultured for 24 h prior to imaging.

Live cell imaging and analysis

Prior to imaging, cells were transferred to video medium (DMEM: F12 without phenol red supplemented with 0.3% glucose, 1× N2, 1× B27 and 1 mM pyruvic acid). Cells were allowed to adapt to the new medium in ambient air for at least 30 min at 37°C. Image acquisition and image analysis were performed on the Cochin Imaging Facility. Image acquisition was done using a Zeiss Axiovert 200 M microscope with oil immersion objective 63×/NA 1.4 in a temperature-controlled CO_2-incubation system. The acquisition sequence was 1 min long, with scans performed every 1 s. Stacks were built using Meta Morph v7.5 (Molecular Devices, Silicon Valley, CA, USA) and analyzed using the IMARIS software (Bitplane, South Windsor, CT, USA). About 100 comets were tracked in each cell, moving straightforward, radially from the centrosome region to the periphery. Instant velocities of comets were measured between each time point and further averaged over their time courses. Independent experiments were repeated at least three times, a total of 8–46 cells were analyzed for each group.

Live cell tracking of lysosome vesicles

Fluorescent staining and confocal microscopy

Acidic vesicles in 2 weeks in vitro confluent mouse astrocytes and 6–10 weeks iPSC-derived human astrocytes culture were loaded with 200 nM Lysotracker Red DND-99 (Invitrogen, Lieden, The Netherlands) in culture medium at 37°C for 1 and 24 h, respectively. Prior to imaging, cells were transferred to video medium. Cells were allowed to adapt to the new medium in ambient air for at least 30 min at 37°C. Image acquisition and image analysis were performed on the Cochin Imaging Facility. Live stained cells were imaged with an inverted confocal microscope (Zeiss Axiovert 200 M) using oil immersion objective 63×/NA 1.4 Lysotracker Red DND-99 (Molecular Probes, Life Technologies). Time-lapse confocal images were acquired every 2 s for 2 min. Stacks were built using Meta Morph v7.5 (Molecular Devices) and analyzed using the IMARIS software (Bitplane). About 100–200 vesicles were tracked in each cell. Independent experiments were repeated at least three times, a total of 15–74 cells were analyzed for each group.

Vesicle tracking and data analysis

Vesicle mobility was analyzed by IMARIS software (Bitplane) to obtain several mobility parameters (34). Briefly, a 2D Gaussian curve was fitted on the selected vesicles in each image within the time series, and the x- and y-coordinates of the peaks of the curves were connected to acquire tracks of vesicle mobility (trajectories). The current time (time from the beginning of single vesicle tracking), displacement length (distance between the first and last spot position) and track length (TL, the total length of the analyzed vesicle pathway) were determined and the ratio of the displacement, meaning the distance between the first and the last spot position, over the total track length of each mobile vesicle were measured to analyze vesicle directionality.

EpoD or vehicle treatment of Mecp2[308/y] and wild-type mice

Groups (n = 7–10) of 5-week-old male *Mecp*[308/y] mice or 5-week-old wild-type littermates were administered weekly intraperitoneal injections of 1 mg/kg EpoD, or vehicle (DMSO), for a total of 12 consecutive weeks. Experiments have been performed according to guidelines concerning randomization and blinding (56). Treatment continued throughout behavioral testing. We chose to focus on male *Mecp2*[308/y] mice because of the unpredictability of heterozygous females' phenotype deriving from the XCI phenomena and because male mice develop RTT pathology more consistently than females. Indeed, hemizygote male mice allow eliminating the confounding effects of a variable phenotype while investigating the role of Mecp2 gene mutations on the development of RTT-like symptoms. Animals were monitored for signs of abnormal behavior or distress, and were weighed weekly. After 12 weeks of dosing, the mice underwent behavioral testing as described below. To unravel the effects of EpoD treatment on exploratory behavior, mice were tested in the marble-burying test.

Marble-burying test

The mouse Tecniplast cages were filled with ∼5 cm of sawdust bedding, lightly tamped down to make a flat, even surface over which nine marbles were evenly distributed. At the end of a 10 min session during which mice were allowed to freely explore the cage, the number of buried marbles (at least 2/3 of their depth) was counted. The test was carried out under dim lights.

Data analysis

Parametric analyses of variance (ANOVA) were performed on all mice behavior data. Specifically, ANOVA model included genotype as between-subject factor and one or two repeated measures factors. Post hoc comparisons were performed using Tukey's test, which can be used in the absence of significant ANOVA results. The Mann–Whitney *U*-test was applied on latency data that had no normal distribution. Molecular data were analyzed by Student's *t*-test for quantitative data. A *P*-value of <0.05 was considered statistically significant. Statistical analyses were performed using GraphPad Prism 5 (GraphPad Software, La Jolla, CA, USA).

Supplementary Material

Supplementary Material is available at *HMG* online.

Acknowledgements

Funding

References

1. Hagberg, B., Hanefeld, F., Percy, A. and Skjeldal, O. (2002) An update on clinically applicable diagnostic criteria in Rett syndrome. Comments to Rett Syndrome Clinical Criteria Consensus Panel Satellite to European Paediatric Neurology Society Meeting, Baden Baden, Germany, 11 September 2001. *Eur. J. Paediatr. Neurol.*, **6**, 293–297.

2. Bienvenu, T. and Chelly, J. (2006) Molecular genetics of Rett syndrome: when DNA methylation goes unrecognized. *Nat. Rev. Genet.*, **7**, 415–426.

3. Amir, R.E., Van den Veyver, I.B., Wan, M., Tran, C.Q., Francke, U. and Zoghbi, H.Y. (1999) Rett syndrome is caused by mutations in X-linked MECP2, encoding methyl-CpG-binding protein 2. *Nat. Genet.*, **23**, 185–188.

4. Chahrour, M. and Zoghbi, H.Y. (2007) The story of Rett syndrome: from clinic to neurobiology. *Neuron*, **56**, 422–437.

5. Guy, J., Cheval, H., Selfridge, J. and Bird, A. (2011) The role of MeCP2 in the brain. *Annu. Rev. Cell Dev. Biol.*, **27**, 631–652.

6. Shahbazian, M., Young, J., Yuva-Paylor, L., Spencer, C., Antalffy, B., Noebels, J., Armstrong, D., Paylor, R. and Zoghbi, H. (2002) Mice with truncated MeCP2 recapitulate many Rett syndrome features and display hyperacetylation of histone H3. *Neuron*, **35**, 243–254.

7. Moretti, P., Bouwknecht, J.A., Teague, R., Paylor, R. and Zoghbi, H.Y. (2005) Abnormalities of social interactions and homecage behavior in a mouse model of Rett syndrome. *Hum. Mol. Genet.*, **14**, 205–220.

8. Moretti, P., Levenson, J.M., Battaglia, F., Atkinson, R., Teague, R., Antalffy, B., Armstrong, D., Arancio, O., Sweatt, J.D. and Zoghbi, H.Y. (2006) Learning and memory and synaptic plasticity are impaired in a mouse model of Rett syndrome. *J. Neurosci.*, **26**, 319–327.

9. De Filippis, B., Nativio, P., Fabbri, A., Ricceri, L., Adriani, W., Lacivita, E., Leopoldo, M., Passarelli, F., Fuso, A. and Laviola, G. (2014) Pharmacological stimulation of the brain serotonin receptor 7 as a novel therapeutic approach for Rett syndrome. *Neuropsychopharmacology*, **39**, 2506–2518.

10. Marchetto, M.C., Carromeu, C., Acab, A., Yu, D., Yeo, G.W., Mu, Y., Chen, G., Gage, F.H. and Muotri, A.R. (2010) A model for neural development and treatment of Rett syndrome using human induced pluripotent stem cells. *Cell*, **143**, 527–539.

11. Kim, K.Y., Hysolli, E. and Park, I.H. (2011) Neuronal maturation defect in induced pluripotent stem cells from patients with Rett syndrome. *Proc. Natl Acad. Sci. USA*, **108**, 14169–14174.

12. Ananiev, G., Williams, E.C., Li, H. and Chang, Q. (2011) Isogenic pairs of wild type and mutant induced pluripotent stem cell (iPSC) lines from Rett syndrome patients as in vitro disease model. *PLoS One*, **6**, e25255.

13. Farra, N., Zhang, W.B., Pasceri, P., Eubanks, J.H., Salter, M.W. and Ellis, J. (2012) Rett syndrome induced pluripotent stem cell-derived neurons reveal novel neurophysiological alterations. *Mol. Psychiatry*, **17**, 1261–1271.

14. Cheung, A.Y., Horvath, L.M., Carrel, L. and Ellis, J. (2012) X-chromosome inactivation in rett syndrome human induced pluripotent stem cells. *Front. Psychiatry*, **3**, 24.

15. Larimore, J., Ryder, P.V., Kim, K.Y., Ambrose, L.A., Chapleau, C., Calfa, G., Gross, C., Bassell, G.J., Pozzo-Miller, L., Smith, Y. *et al.* (2013) MeCP2 regulates the synaptic expression of a Dysbindin-BLOC-1 network component in mouse brain and human induced pluripotent stem cell-derived neurons. *PLoS One*, **8**, e65069.

16. Tanaka, Y., Kim, K.Y., Zhong, M., Pan, X., Weissman, S.M. and Park, I.H. (2014) Transcriptional regulation in pluripotent stem cells by methyl CpG-binding protein 2 (MeCP2). *Hum. Mol. Genet.*, **23**, 1045–1055.

17. Williams, E.C., Zhong, X., Mohamed, A., Li, R., Liu, Y., Dong, Q., Ananiev, G.E., Mok, J.C., Lin, B.R., Lu, J. *et al.* (2014) Mutant astrocytes differentiated from Rett syndrome patients-specific iPSCs have adverse effects on wild-type neurons. *Hum. Mol. Genet.*, **23**, 2968–2980.

18. Djuric, U., Cheung, A.Y., Zhang, W., Mok, R.S., Lai, W., Piekna, A., Hendry, J.A., Ross, P.J., Pasceri, P., Kim, D.S. *et al.* (2015) MECP2e1 isoform mutation affects the form and function of neurons derived from Rett syndrome patient iPS cells. *Neurobiol. Dis.*, **76**, 37–45.

19. Livide, G., Patriarchi, T., Amenduni, M., Amabile, S., Yasui, D., Calcagno, E., Lo Rizzo, C., De Falco, G., Ulivieri, C., Ariani, F. *et al.* (2015) GluD1 is a common altered player in neuronal differentiation from both MECP2-mutated and CDKL5-mutated iPS cells. *Eur. J. Hum. Genet.*, **23**, 195–201.

20. Ballas, N., Lioy, D.T., Grunseich, C. and Mandel, G. (2009) Non-cell autonomous influence of MeCP2-deficient glia on neuronal dendritic morphology. *Nat. Neurosci.*, **12**, 311–317.

21. Liu, H. and Zhang, S.C. (2011) Specification of neuronal and glial subtypes from human pluripotent stem cells. *Cell. Mol. Life Sci.*, **68**, 3995–4008.

22. Maezawa, I., Swanberg, S., Harvey, D., LaSalle, J.M. and Jin, L.W. (2009) Rett syndrome astrocytes are abnormal and spread MeCP2 deficiency through gap junctions. *J. Neurosci.*, **29**, 5051–5061.

23. Okabe, Y., Takahashi, T., Mitsumasu, C., Kosai, K., Tanaka, E. and Matsuishi, T. (2012) Alterations of gene expression and glutamate clearance in astrocytes derived from an MeCP2-null mouse model of Rett syndrome. *PLoS One*, **7**, e35354.

24. Lioy, D.T., Garg, S.K., Monaghan, C.E., Raber, J., Foust, K.D., Kaspar, B.K., Hirrlinger, P.G., Kirchhoff, F., Bissonnette, J.M., Ballas, N. *et al.* (2011) A role for glia in the progression of Rett's syndrome. *Nature*, **475**, 497–500.

25. LeDizet, M. and Piperno, G. (1987) Identification of an acetylation site of Chlamydomonas alpha-tubulin. *Proc. Natl Acad. Sci. USA*, **84**, 5720–5724.

26. Palazzo, A., Ackerman, B. and Gundersen, G.G. (2003) Cell biology: tubulin acetylation and cell motility. *Nature*, **421**, 230.

27. Delépine, C., Nectoux, J., Bahi-Buisson, N., Chelly, J. and Bienvenu, T. (2013) MeCP2 deficiency is associated with impaired microtubule stability. *FEBS Lett.*, **587**, 245–253.

28. Gold, W.A., Lacina, T.A., Cantrill, L.C. and Christodoulou, J. (2015) MeCP2 deficiency is associated with reduced levels of tubulin acetylation and can be restored using HDAC6 inhibitors. *J. Mol. Med. (Berl)*, **93**, 63–72.

29. Roux, J.C., Zala, D., Panayotis, N., Borges-Correia, A., Saudou, F. and Villard, L. (2012) Modification of Mecp2 dosage alters axonal transport through the Huntingtin/Hap1 pathway. *Neurobiol. Dis.*, **45**, 786–795.

30. Nectoux, J., Florian, C., Delepine, C., Bahi-Buisson, N., Khelfaoui, M., Reibel, S., Chelly, J. and Bienvenu, T. (2012) Altered microtubule dynamics in Mecp2-deficient astrocytes. *J. Neurosci. Res.*, **90**, 990–998.

31. Krencik, R. and Zhang, S.C. (2011) Directed differentiation of functional astroglial subtypes from human pluripotent stem cells. *Nat. Protoc.*, **6**, 1710–1717.

32. Stepanova, T., Slemmer, J., Hoogenraad, C.C., Lansbergen, G., Dortland, B., De Zeeuw, C.I., Grosveld, F., van Cappellen, G., Akhmanova, A. and Galjart, N. (2003) Visualization of microtubule growth in cultured neurons via the use of EB3-GFP (end-binding protein 3-green fluorescent protein). *J. Neurosci.*, **23**, 2655–2664.

33. Zilberman, Y., Ballestrem, C., Carramusa, L., Mazitschek, R., Khochbin, S. and Bershadsky, A. (2009) Regulation of microtubule dynamics by inhibition of the tubulin deacetylase HDAC6. *J. Cell. Sci.*, **122**, 3531–3541.

34. Potokar, M., Kreft, M., Pangrsic, T. and Zorec, R. (2005) Vesicle mobility studied in cultured astrocytes. *Biochem. Biophys. Res. Commun*, **329**, 678–683.

35. Stenovec, M., Milosevic, M., Petrusic, V., Potokar, M., Stevic, Z., Prebil, M., Kreft, M., Trkov, S., Andjus, P.R. and Zorec, R. (2011) Amyotrophic lateral sclerosis immunoglobulins G enhance the mobility of Lysotracker-labelled vesicles in cultured rat astrocytes. *Acta Physiol. (Oxf)*, **203**, 457–471.

36. Brunden, K.R., Zhang, B., Carroll, J., Yao, Y., Potuzak, J.S., Hogan, A.M., Iba, M., James, M.J., Xie, S.X., Ballatore, C. *et al.* (2010) Epothilone D improves microtubule density, axonal integrity, and cognition in a transgenic mouse model of tauopathy. *J. Neurosci.*, **30**, 13861–13866.

37. Brunden, K.R., Yao, Y., Potuzak, J.S., Ferrer, N.I., Ballatore, C., James, M.J., Hogan, A.M., Trojanowski, J.Q., Smith, A.B. 3rd and Lee, V.M. (2011) The characterization of microtubule-stabilizing drugs as possible therapeutic agents for Alzheimer's disease and related tauopathies. *Pharmacol. Res.*, **63**, 341–351.

38. Reed, N.A., Cai, D., Blasius, T.L., Jih, G.T., Meyhofer, E., Gaertig, J. and Verhey, K.J. (2006) Microtubule acetylation promotes kinesin-1 binding and transport. *Curr. Biol.*, **16**, 2166–2172.

39. Bulinski, J.C. (2007) Microtubule modification: acetylation speeds anterograde traffic flow. *Curr. Biol.*, **17**, R18–R20.

40. Dompierre, J.P., Godin, J.D., Charrin, B.C., Cordelieres, F.P., King, S.J., Humbert, S. and Saudou, F. (2007) Histone deacetylase 6 inhibition compensates for the transport deficit in Huntington's disease by increasing tubulin acetylation. *J. Neurosci.*, **27**, 3571–3583.

41. Hubbert, C., Guardiola, A., Shao, R., Kawaguchi, Y., Ito, A., Nixon, A., Yoshida, M., Wang, X.F. and Yao, T.P. (2002) HDAC6 is a microtubule-associated deacetylase. *Nature*, **417**, 455–458.

42. Matsuyama, A., Shimazu, T., Sumida, Y., Saito, A., Yoshimatsu, Y., Seigneurin-Berny, D., Osada, H., Komatsu, Y., Nishino, N., Khochbin, S. *et al.* (2002) In vivo destabilization of dynamic microtubules by HDAC6-mediated deacetylation. *EMBO J.*, **21**, 6820–6831.

43. North, B.J., Marshall, B.L., Borra, M.T., Denu, J.M. and Verdin, E. (2003) The human Sir2 ortholog, SIRT2, is an NAD+-dependent tubulin deacetylase. *Mol. Cell.*, **11**, 437–444.

44. Potokar, M., Kreft, M., Li, L., Daniel Andersson, J., Pangrsic, T., Chowdhury, H.H., Pekny, M. and Zorec, R. (2007) Cytoskeleton and vesicle mobility in astrocytes. *Traffic*, **8**, 12–20.

45. Xu, X., Kozikowski, A.P. and Pozzo-Miller, L. (2014) A selective histone deacetylase-6 inhibitor improves BDNF trafficking in hippocampal neurons from Mecp2 knockout mice: implications for Rett syndrome. *Front. Cell. Neurosci.*, **8**, 68.

46. Andrieux, A., Salin, P., Schweitzer, A., Begou, M., Pachoud, B., Brun, P., Gory-Faure, S., Kujala, P., Suaud-Chagny, M.F., Hofle, G. *et al.* (2006) Microtubule stabilizer ameliorates synaptic function and behavior in a mouse model for schizophrenia. *Biol. Psychiatry*, **60**, 1224–1230.

47. Zhang, B., Carroll, J., Trojanowski, J.Q., Yao, Y., Iba, M., Potuzak, J.S., Hogan, A.M., Xie, S.X., Ballatore, C., Smith, A.B. 3rd *et al.* (2012) The microtubule-stabilizing agent, epothilone D, reduces axonal dysfunction, neurotoxicity, cognitive deficits, and Alzheimer-like pathology in an interventional study with aged tau transgenic mice. *J. Neurosci.*, **32**, 3601–3611.

48. Beer, T.M., Higano, C.S., Saleh, M., Dreicer, R., Hudes, G., Picus, J., Rarick, M., Fehrenbacher, L. and Hannah, A.L. (2007) Phase II study of KOS-862 in patients with metastatic androgen independent prostate cancer previously treated with docetaxel. *Invest. New Drugs*, **25**, 565–570.

49. Bedard, P.L., Di Leo, A. and Piccart-Gebhart, M.J. (2010) Taxanes: optimizing adjuvant chemotherapy for early-stage breast cancer. *Nat. Rev. Clin. Oncol.*, **7**, 22–36.

50. Lee, C.B., Wu, Z., Zhang, F., Chappell, M.D., Stachel, S.J., Chou, T.C., Guan, Y. and Danishefsky, S.J. (2001) Insights into long-range structural effects on the stereochemistry of aldol condensations: a practical total synthesis of desoxyepothilone F. *J. Am. Chem. Soc.*, **123**, 5249–5259.

51. Rivkin, A., Yoshimura, F., Gabarda, A.E., Cho, Y.S., Chou, T.C., Dong, H. and Danishefsky, S.J. (2004) Discovery of (E)-9,10-dehydroepothilones through chemical synthesis: on the emergence of 26-trifluoro-(E)-9,10-dehydro-12,13-desoxyepothilone B as a promising anticancer drug candidate. *J. Am. Chem. Soc.*, **126**, 10913–10922.

52. Gebicke-Haerter, P.J., Bauer, J., Schobert, A. and Northoff, H. (1989) Lipopolysaccharide-free conditions in primary astrocyte cultures allow growth and isolation of microglial cells. *J. Neurosci.*, **9**, 183–194.

53. Emdad, L., D'Souza, S.L., Kothari, H.P., Qadeer, Z.A. and Germano, I.M. (2012) Efficient differentiation of human embryonic and induced pluripotent stem cells into functional astrocytes. *Stem Cells Dev.*, **21**, 404–410.

54. Allen, R.C., Zoghbi, H.Y., Moseley, A.B., Rosenblatt, H.M. and Belmont, J.W. (1992) Methylation of HpaII and HhaI sites near the polymorphic CAG repeat in the human androgen-receptor gene correlates with X chromosome inactivation. *Am. J. Hum. Genet.*, **51**, 1229–1239.

55. Griscelli, F., Feraud, O., Oudrhiri, N., Gobbo, E., Casal, I., Chomel, J.C., Bieche, I., Duvillard, P., Opolon, P., Turhan, A.G. *et al.* (2012) Malignant germ cell-like tumors, expressing Ki-1 antigen (CD30), are revealed during in vivo differentiation of partially reprogrammed human-induced pluripotent stem cells. *Am. J. Pathol.*, **180**, 2084–2096.

56. Landis, S.C., Amara, S.G., Asadullah, K., Austin, C.P., Blumenstein, R., Bradley, E.W., Crystal, R.G., Darnell, R.B., Ferrante, R. J., Fillit, H. *et al.* (2012) A call for transparent reporting to optimize the predictive value of preclinical research. *Nature*, **490**, 187–191.